THE JOURNAL OF PHYSICAL CHEMISTRY LETTERS
A JOURNAL OF THE AMERICAN CHEMICAL SOCIETY

pubs.acs.org/JPCL

Letter

Near-Infrared Absorption Features of Triplet-Pair States Assigned by Photoinduced-Absorption-Detected Magnetic Resonance

Ryan D. Dill, Gajadhar Joshi, Karl J. Thorley, John E. Anthony, Brian Fluegel, Justin C. Johnson, and Obadiah G. Reid*

Cite This: *J. Phys. Chem. Lett.* 2023, 14, 2387−2394

Read Online

ACCESS | Metrics & More | Article Recommendations | Supporting Information

ABSTRACT: Singlet fission proceeds through a manifold of triplet-pair states that are exceedingly difficult to distinguish spectroscopically. Here, we introduce a new implementation of photoinduced-absorption-detected magnetic resonance (PADMR) and use it to understand the excited-state absorption spectrum of a tri-2-pentylsilylethynyl pentadithiophene (TSPS-PDT) film. These experiments allow us to directly correlate magnetic transitions driven by RF with electronic transitions in the visible and near-infrared spectrum with high sensitivity. We find that the new near-infrared excited-state transitions that arise in thin films of TSPS-PDT are correlated with the magnetic transitions of T_1, not ^{5}TT. Thus, we assign these features to the excited-state absorption of ^{1}TT, which is depleted when T_1 states are driven to a spin configuration that forbids subsequent fusion. These results clarify the disputed origin of triplet-associated near-infrared absorption features in singlet-fission materials and demonstrate an incisive general purpose tool for studying the evolution of high-spin excited states.

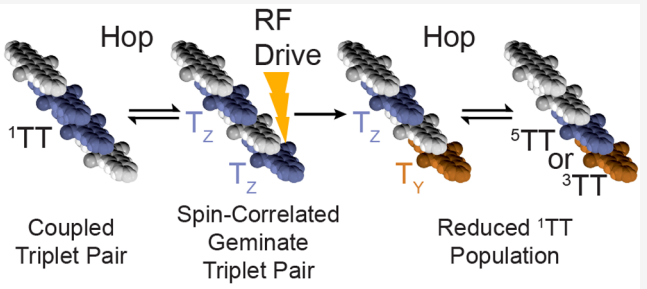

Singlet fission (SF) is a multiexciton generation process wherein a singlet excited state on one chromophore, S_1, partitions its energy with a nearby chromophore in its ground state, S_0, to generate two triplet excited states, $T_1 + T_1$. As a downconversion process, SF can be used in photovoltaics to reduce thermalization losses,[1−3] but recent work has also suggested that intermediate triplet-pair states, particularly ^{5}TT, may have quantum information (QI) applications,[4−8] since these may form with high initial spin polarization. Distinct pair states, ^{n}TT, form when two adjacent triplet states experience a strong interchromophore exchange interaction, such that pairs with different spin multiplicities, n = 1, 3, or 5, possess different energies. Although SF initially proceeds through spin-allowed interconversion to ^{1}TT, the net-triplet and net-quintet states, ^{3}TT and ^{5}TT, often play an important role in the dynamics but are exceedingly difficult to distinguish due to their electronic similarity.

In principle, the intertriplet interactions make the triplet-pair states distinguishable from T_1,[9] but in practice, it is difficult to accurately assign optical absorption features. Here, we introduce a new implementation of photoinduced-absorption-detected magnetic resonance (PADMR) spectroscopy and use it to directly correlate photoinduced absorption spectra with spin transitions to identify the optical contributions of triplet-pair states in a polycrystalline thin film of tri-2-pentylsilylethynyl pentadithiophene (TSPS-PDT; Figure 1).[10,11] PADMR is a type of population-detected magnetic resonance, or magnetic action spectrum—magnetic-sublevel transitions drive changes in an observed electronic-state concentration by modifying one or more electronic-state interconversion rate constant. In the case of PADMR, we measure the change in photoinduced (or excited state) optical absorption of a sample caused by RF- or microwave-induced transitions within the magnetic state manifold. This detection mechanism affords a much more versatile tool than the more commonly employed photoluminescence-detected magnetic resonance (PLDMR), as it can be applied to any system with high-spin excited states, not only those kinetically coupled to luminescent states—a point of particular importance for studying singlet-fission systems, which do not usually emit. Although PADMR experiments have been described before,[12−30] our PADMR spectrometer (diagrammed in Figures 1 and S2) differs markedly. It operates up to very high modulation frequencies (200 MHz) and permits measurements of the PADMR signal as a function of RF-drive frequency (*f*-PADMR), allowing access to short time scales and low (including 0) magnetic fields, in addition to the more

Received: December 1, 2022
Accepted: February 22, 2023
Published: February 27, 2023

https://doi.org/10.1021/acs.jpclett.2c03665
J. Phys. Chem. Lett. 2023, 14, 2387−2394

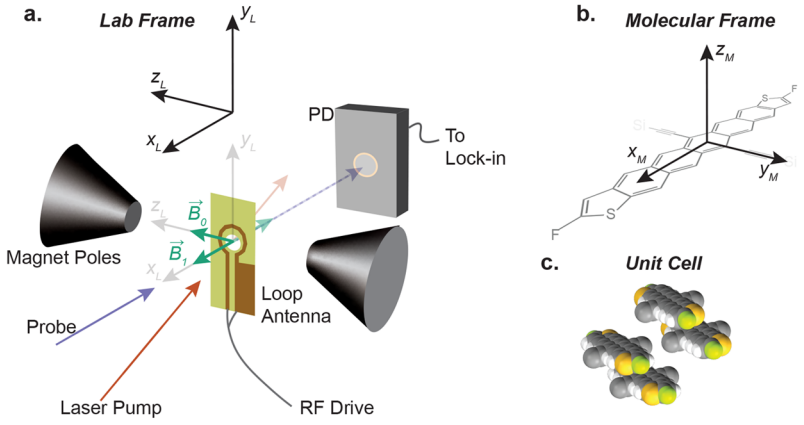

Figure 1. The PADMR spectrometer. (a) Lab-frame view of the PADMR spectrometer. The sample is mounted to a PCB loop antenna, inside an optical cryostat, between the pole tips of an electromagnet. The probe beam passes through the center of the RF antenna, and its intensity is measured by a photodetector. A laser is overlapped with the probe. For PA experiments, only the laser is modulated. For PADMR experiments, only the RF is modulated. See SI section S1.2 for details. (b) The molecular reference frame commonly used for acenes is assumed valid here.[33] (c) The unit-cell for crystallites of TSPS-PDT, first reported in ref 10, is reproduced here. The reduced symmetry of TSPS-PDT, relative to standard acenes, means that there are four unique nearest-neighbor-pair conformations, two of which are shown. To aid in visualization, the trialkylsilyl substituents are not included.

common scan variables, probe wavelength (λ-PADMR) and magnetic field (B-PADMR).[17,19] Especially for disordered samples, f-PADMR at zero magnetic field offers strong signals, good spectral resolution, and extremely simple interpretation. In addition, advances in available computer equipment in the 10−20 years since this technique was regularly used have allowed us to implement powerful 2D scan modes for correlating different scan variables that have not been previously demonstrated. See the Supporting Information section S1 for full experimental details. Applying this powerful tool to thin films of TSPS-PDT reveals strong magnetic resonance (MR) transitions associated with free triplet, T_1, and weak MR transitions associated with small populations in ^{5}TT. Importantly, the photoinduced absorption features in the near-infrared (NIR), which do not appear in solution and have been commonly assigned to triplet-pair states,[9,10,31,32] are correlated with transitions in T_1. This surprising observation is most likely explained by kinetic coupling between T_1 and the magnetically dark ^{1}TT state via recombination of spin-correlated geminate triplet pairs—leading us to assign the NIR PA features observed here to ^{1}TT.

We begin by discussing the photoinduced absorption (PA) spectroscopy of TSPS-PDT films, as it is essential background for understanding the PADMR results. PA spectroscopy probes the system's *electronic* dynamics under modulated visible light excitation, or pump, and is the frequency-domain analog to pulsed-beam transient absorption spectroscopy, more typically carried out in the time-domain. For details on the experimental setup and interpretation, see the Supporting Information section S1.

PA features of TSPS-PDT. Figure 2a shows the absorption spectrum of a TSPS-PDT film at room temperature. Like the one in ref 10, it is red-shifted and broadened relative to the solution-phase absorption due to strong interchromophore interactions. Figure 2b shows the PA spectrum for the same sample, the lock-in signal associated with an amplitude-modulated laser pump recorded as a function of probe wavelength (temperature ≈ 5−10 K, 642 nm excitation, 1 kHz laser-modulation frequency, f_{mod}^{opt}). It is similar to the transient absorption spectra in ref 10, showing a ground-state bleach

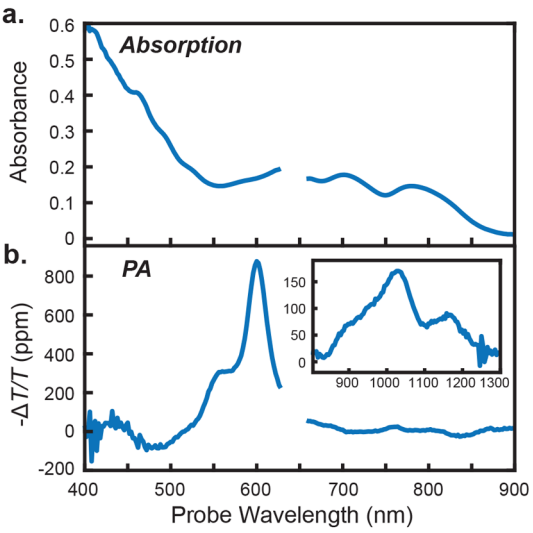

Figure 2. Steady-state and photoinduced absorption spectra for a TSPS-PDT film. (a) Absorption spectrum ($-\log(T/T_0)$) measured at room temperature with the experimental setup described in the text. A constant value (0.25) was subtracted to correct for scattering. The gap in the spectrum is where the notch filter absorbs. (b) The PA spectrum (642 nm pump wavelength, pump intensity ≈ 2 W/cm^2, f_{mod}^{opt} = 1 kHz, temperature ≈ 5−10 K) shows strong absorption peaking at 595 nm, associated with triplet states. The modulation frequency, f_{mod}^{opt} = 1 kHz, is low, so the spectrum approximately represents steady-state PA. This spectrum has been rephased by ϕ = +22.9° to put most of the signal into a single channel (the rephasing process is discussed in section S1.2.5). Inset: PA signals in the NIR are also clear. Experimental parameters for both data sets are the same, except that an 800 nm long-pass filter was added for the NIR data. This spectrum has been rephased by ϕ = −70°.

(GSB) near 500 nm, strong PA features with partially resolved vibronic progression from 550 to 650 nm, and PA in the NIR from 900 to 1200 nm. The additional GSB features are more difficult to discern but appear as weak dips in the spectrum around 725 and 840 nm. Reduced ground-state absorption around 750 nm appears as a small hump in the PA spectrum.

https://doi.org/10.1021/acs.jpclett.2c03665
J. Phys. Chem. Lett. 2023, 14, 2387−2394

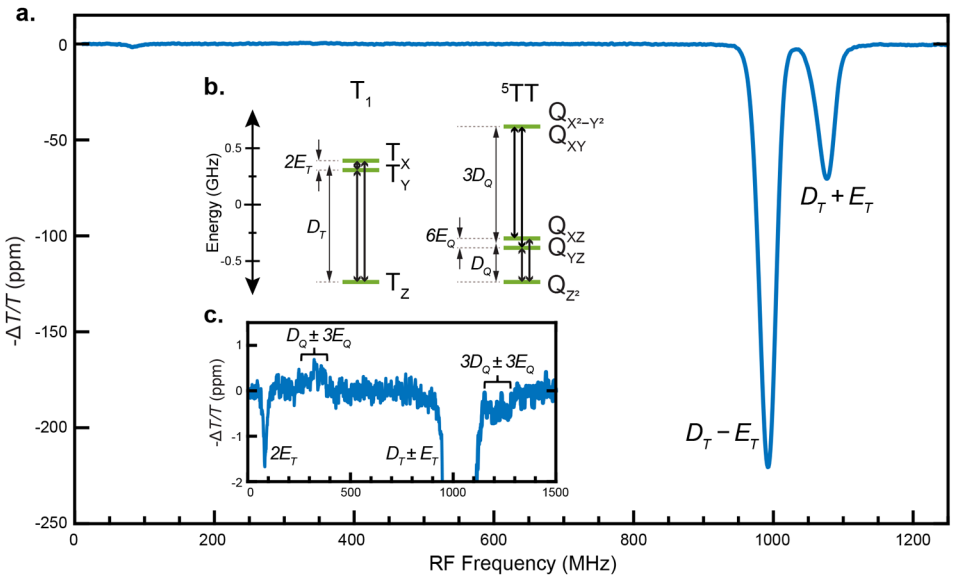

Figure 3. The PADMR spectrum of TSPS-PDT is dominated by triplet signatures. (a) Detecting at the triplet PA's peak, the *f*-PADMR spectrum of a TSPS-PDT film shows three main peaks (85, 990, and 1077 MHz), corresponding to transitions within the triplet manifold, T_1 (600 nm probe, 642 nm continuous pump, pump intensity ≈ 15 W/cm^2, 2.99 kHz RF-modulation frequency, zero magnetic field, temperature ≈ 5−10 K). The negative signals indicate that PA intensity is reduced by RF drive. These data have been rephased by ϕ = +29.8° to maximize the amplitude in a single channel (the rephasing process is discussed in SI sections S1.2.5 and S1.2.6). (b) Sublevel energy diagram for T_1 (left) and ^{5}TT (right) in the zero-field basis. Arrows show observed transitions. The T_1 splittings are from a fit, with $|D_T|$ = 1033 MHz and $|E_T|$ = 41.6 MHz. The ^{5}TT sublevels are named as in ref 4, and the splittings shown disregard anisotropic exchange.[34] (c) Much weaker features are assigned to quintet transitions.

The slight mismatch between steady-state absorption features and their corresponding PA features likely comes from the different temperatures used and site selectivity in the PA data due to laser photoexcitation. The vibronic progression peaking at 600 nm is typical of triplet-containing states in PDT films but does not easily distinguish T_1 from the various triplet-pair states. The NIR PA features were previously attributed to triplet-pair states, based largely on their absence in solution-phase triplet spectra;[10] their assignment is discussed further below.

Under conditions of low pump-modulation frequency, f_{mod}^{opt}, such as in Figure 2b, the signal is dominated by species with long lifetimes. At higher f_{mod}^{opt}, those signals are diminished—measuring the PA spectrum as a function of f_{mod}^{opt} informs on electronic dynamics (Figures S10 and S11). Reproducing the entire modulation frequency dependence for TSPS-PDT requires at least five decay time constants. The longest three lifetimes ($\tau_{1,2,3}$ = 94, 42, and 3.5 μs) are all associated with very similar optical spectra (see SI Figures S11 and S12). The strong similarity in the PA spectra associated with these three time constants (SI Figure S12) suggests they are all associated with triplet-*containing* states (i.e., T_1 or ^{n}TT). The remaining signal at high f_{mod}^{opt} is described by two time constants, $\tau_{4,5}$ = 430 and 1.8 ns; these time constants are associated with very different spectral shapes, dominated by broad indistinct PIA overlapping with sharp GSB features. The 1.8 ns time constant is probably related to the instrument bandwidth limit and therefore serves as an upper bound on the corresponding state lifetime. The observed lifetimes of all states depend on pump intensity and applied magnetic field (see SI Figures S13−S15). They are also much longer than those reported in ref 10, most likely due to the much lower temperatures used here (~10 vs 300 K). Specific assignment of the two short-lived spectra (430 and 1.8 ns decay times) is not immediately clear and will require further investigation, as they do not resemble anything from our prior room-temperature TA studies.[10] We thus focus the remainder of the discussion on the long-lived species observed at low pump-modulation frequencies.

As in prior transient absorption studies, the PA dynamics and spectra alone cannot be used to assign the features we observe to specific magnetic species. We turn to PADMR spectroscopy to directly correlate electronic transitions with the magnetic transitions to which they are kinetically coupled, in particular the NIR PIA features from 900 to 1200 nm.

Free triplet signatures in f-PADMR. The *f*-PADMR spectrum of TSPS-PDT probed at the typical triplet PA feature (600 nm) at zero magnetic field (RF-modulation frequency, f_{mod}^{RF} = 2.99 kHz) is shown in Figure 3a. The three strongest features at 85, 990, and 1077 MHz are associated with transitions between sublevels of a triplet state, which we characterize in terms of its zero-field splitting parameters, D and E.[35] A fit gives $|D|$ = 1033 MHz and $|E|$ = 41.6 MHz (Figure S16).

The simplest assignment of these magnetic transitions is to T_1, corresponding to $2E_T$, $D_T - E_T$, and $D_T + E_T$. While ^{3}TT and ^{5}TT are expected to show transitions at similar frequencies (Figure 3b) major contributions from these species can be ruled out. It is unlikely that the observed peaks are primarily composed of ^{5}TT transitions because ^{5}TT typically displays comparably strong MR features at intermediate frequencies, corresponding to $Q_{Z^2} \leftrightarrow Q_{YZ}$ and $Q_{Z^2} \leftrightarrow Q_{XZ}$. Transitions at such frequencies *are* observed (Figure 3c; see below) but are orders of magnitude weaker. Assignment of the strong features to ^{3}TT is similarly unlikely, though it cannot be distinguished on the basis of the spectra. ^{3}TT is expected to decay via the spin-allowed "triplet-channel annihilation" (TCA) pathway, $^3\text{TT} \rightarrow T_1 + S_0$[36−39] and is unlikely to form with high yield to begin with due to symmetry considerations.[4,34,36,40]

The PADMR signals in Figure 3a are negative, $-\Delta T/T < 0$, indicating that driving these MR transitions *reduces* photo-induced absorption, corresponding to a reduced concentration

https://doi.org/10.1021/acs.jpclett.2c03665
J. Phys. Chem. Lett. 2023, 14, 2387−2394

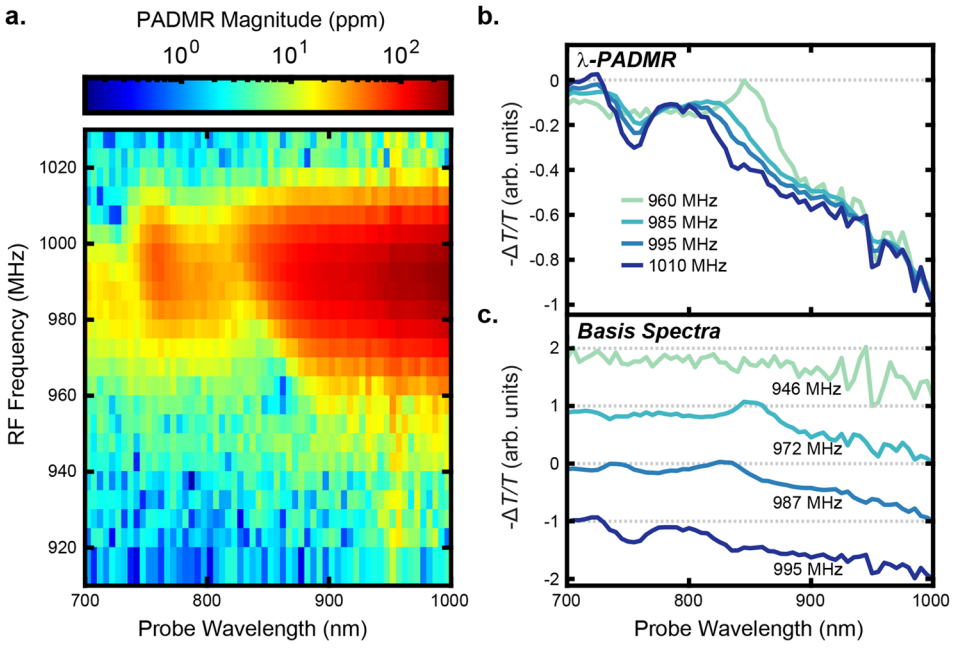

Figure 4. $f \times \lambda$-PADMR correlates near-IR PA with T_1 MR. (a) The PADMR signal magnitude, $R = \frac{\sqrt{X^2 + Y^2}}{T}$, shows strong signals when probing the 1000 nm PA (Figure 2) and driving the $T_Z \leftrightarrow T_Y$ transition (642 nm pump wavelength, pump intensity ≈ 15 W/cm^2, f^{RF}_{mod} = 2.99 kHz, temperature ≈ 5−10 K). Slight asymmetry shows that the PA and MR spectral positions are correlated. (b) λ-PADMR spectra demonstrate shifting PA intensity as a function of f^{RF}_{Drive}. They are slices taken from a global fit of the phase-optimized PADMR data (applied phase, ϕ = +34.2°; see SI section S1.2.5 for a discussion of the rephasing process). (c) The λ-PADMR basis spectra obtained by the fit. All are most intense near 1000 nm. A superimposed positive feature is seen at 850 nm when driven by 972 MHz RF and likely corresponds to a GSB (RF increases ground-state population). It shifts to bluer wavelengths with increasing f^{RF}_{Drive}. A similar shift is seen in a GSB near 740 nm, and pronounced shifts are seen when probing near the 600 nm PA (SI section S2.3.1).

of the probed state(s). In general, this is caused by sublevel-dependent dynamics, such as a faster decay rate in the product sublevel. The specific origins of the negative PADMR signal are discussed below.

Further interpretation of peak amplitudes in Figure 3 is not straightforward for several reasons. Even the *relative* peak amplitudes are complicated functions of all the dynamical processes with magnetic-sublevel-dependent electronic-state interconversion rates—they are not simply proportional to sublevel population differences; they may be distorted by instrument sensitivity that varies with RF-drive frequency, f^{RF}_{Drive} (see SI section 2.3.4). They may also depend on crystallite orientation bias. The last point is an important nuance: although the transition *frequencies* of a triplet state do not depend on molecular orientation at zero magnetic field, their relative intensities do. Each transition is polarized along a different molecular axis;[41,42] their intensities depend on their projection onto the driving RF magnetic field, B_1.

Weak ^{5}TT transitions in the f-PADMR spectrum. Closer inspection of the *f*-PADMR spectrum (Figure 3c) reveals weak positive features at 250−400 MHz and negative ones at 1150−1250 MHz; we assign these to ^{5}TT. The 250−400 MHz features correspond to $Q_{Z^2} \leftrightarrow Q_{YZ}$ and $Q_{Z^2} \leftrightarrow Q_{XZ}$ (Figure 3b). Those transitions are characteristic of ^{5}TT, since they are centered at $D_Q \approx D_T/3$, where D_Q is the zero-field splitting parameter for ^{5}TT.[34,43,44]

We assign the 1150−1250 MHz features to the four transitions that couple Q_{YZ} and Q_{XZ} to $Q_{X^2-Y^2}$ and Q_{XY}. This assignment is implied by their similar amplitudes compared to the 250−400 MHz features and supported by the slight shift relative to the T_1 features. The relationships between the ^{5}TT and T_1 zero-field splitting parameters, $D_Q = D_T/3$ and $E_Q = E_T/3$, are only exact when the isotropic exchange, J_{TT}, is the only interaction between the two triplets. In real systems, sublevel energies are also affected by anisotropic interactions; for triplet-pairs, the most important is the magnetic dipole−dipole interaction, analogous to the zero-field splitting but between the triplets in the pair.[8,34,43−45] Although we have assigned the weak features to groups of quintet transitions, their low signal-to-noise ratio precludes a more specific and quantitative assignment.

It is clear from these experiments that both T_1 and ^{5}TT are populated by photoexcitation, as detected using the 600 nm PA feature commonly associated with the net-triplet population. In what follows, we turn to the NIR PA feature at 1000 nm, seeking to clarify its assignment and take advantage of its electronic-state specificity.

NIR PA correlates with T_1 MR. In Figure 4, we show PADMR data for TSPS-PDT for the region surrounding the $T_Z \leftrightarrow T_Y$ transition. Figure 4a shows the signal magnitude as a function of both f^{RF}_{Drive} and probe wavelength. Vertical slices in the pseudocolor plot correspond to *f*-PADMR spectra at fixed probe wavelengths; horizontal slices are λ-PADMR spectra at fixed RF-drive frequencies. Figure 4b shows λ-PADMR spectra for selected RF-drive frequencies, extracted from a global fit reconstruction of the phase-optimized PADMR signal ($\frac{-X'}{T}$, where X' is the real part of the complex-valued signal after rephasing; see SI section S1.2.5 for a discussion of the rephasing process). Figure 4c shows the λ-PADMR basis spectra used to model the full data; each is associated with a

https://doi.org/10.1021/acs.jpclett.2c03665
J. Phys. Chem. Lett. 2023, 14, 2387−2394

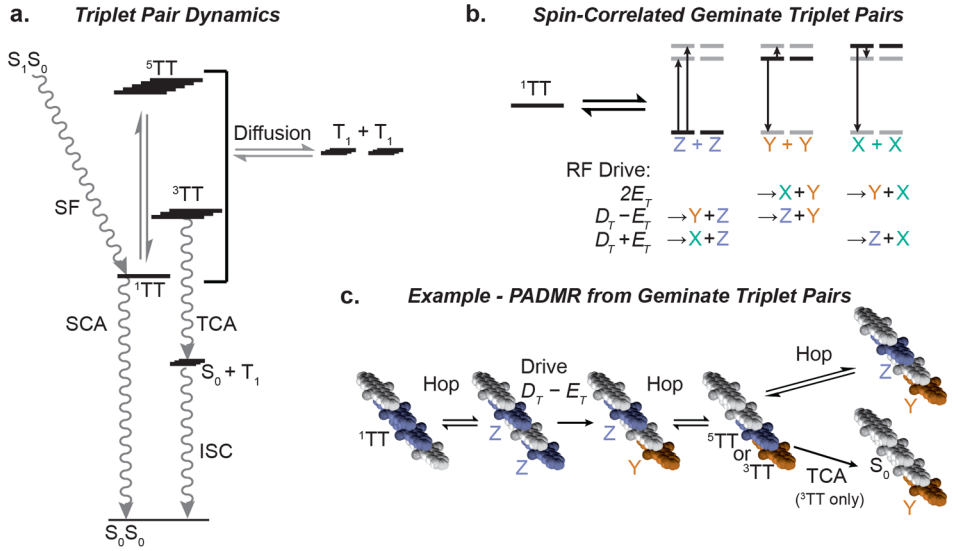

Figure 5. Triplet-pair model for low-temperature TSPS-PDT films. (a) Dynamical model showing triplet-pair formation (SF), diffusion, and deactivation via singlet-channel and triplet-channel annihilation (SCA and TCA), T_1 deactivation through intersystem crossing (ISC), and $^1TT \rightleftharpoons {}^5TT$ equilibration (energy gaps are not to scale). Due to a large antiferromagnetic J_{TT},[10] ^5TT forms in low yields. (b) ^1TT dissociation yields either $T_X + T_X$, $T_Y + T_Y$, or $T_Z + T_Z$. X, Y, and Z correspond to T_X, T_Y, and T_Z. RF absorption drives one partner into a different sublevel, preventing reassociation to ^1TT. (c) An example pathway in which geminate triplet pairs produce a PADMR signal. Molecular stacks are extended along the crystal's *a*-axis. ^1TT formation is followed by a hop. Spatial separation electronically decouples the triplets ($J_{TT} \rightarrow 0$), but they remain spin-correlated: here, as $T_Z + T_Z$. Decoupled triplets can absorb RF photons: here, RF with frequency $D_T - E_T$ drives a $T_Z \rightarrow T_Y$ transition. With reassociation, strong electronic coupling returns; the new pair configuration has net-triplet or net-quintet character. Both ^3TT and ^5TT may dissociate again, but ^3TT can also deactivate via TCA.

Gaussian line shape along the *f*-PADMR dimension centered at the labeled frequency.

All of the λ-PADMR spectra in Figure 4b,c show the previously discussed NIR PA (Figure 2b, inset), as their signal continues increasing beyond 1000 nm. The PADMR signal is strongest near f^{RF}_{Drive} = 990 MHz, the $T_Z \leftrightarrow T_Y$ transition, indicating that that the 1000 nm PA belongs to T_1 *or a state kinetically linked to it*. Its negative sign means that driving the transition *reduces* the probed state population. These observations combined with a consideration of past literature strongly suggest we assign the NIR PA feature in TSPS-PDT to ^1TT. Recall that PADMR signals arise through the influence that magnetic transitions have on the concentration of the probed electronic state: the state you drive with RF is not necessarily identical to that you detect electronically—they need only be kinetically coupled in a sublevel-dependent manner. While assignment to T_1 remains possible, ^1TT is more likely in light of prior work. It was previously assigned to a triplet-pair state,[10] and similar features in other acene derivatives have been assigned explicitly to ^1TT based in part on their similarity to other singlet transitions and their absence in solution-phase triplet spectra, wherein isolated chromophores cannot possess energetically accessible ^1TT.[9,31,32] This assignment is discussed more in the Supporting Information. Importantly, it is consistent with a geminate triplet-pair recombination model, which we discuss in the following section.

Spin-correlated geminate triplet pairs. Figure 5a shows an overall kinetic scheme consistent with singlet fission in TSPS-PDT, which has antiferromagnetic TT exchange coupling,[10] including both triplet-pair separation and loss pathways. In general, dissociation of a triplet-pair state produces a geminate pair of triplets, $^1TT \rightarrow T_1 + T_1$. Although electronically decoupled, geminate triplet pairs may remain spin-correlated long after dissociation, especially at low temperatures where spin−lattice relaxation is slow, as illustrated for ^1TT dissociation in Figure 5b,c. These have been previously described for singlet-fission systems, including in one of our own works.[46−48]

The spin correlation within geminate triplet pairs arises from the original coupled-pair (^{m}TT) wave function, which can be represented by linear combinations of zero-field states in the uncoupled pair basis.[34,36,49] If the triplets are on parallel copies of the same chromophore, then $^1TT = 1/\sqrt{3}(|T_XT_X\rangle + |T_YT_Y\rangle + |T_ZT_Z\rangle)$.[34,36,49] Thus, each ^1TT dissociation event should yield two of the same sublevel (Figure 5b), assuming the superposition state decoheres rapidly. In the ensemble, dissociation should yield equal populations in T_X, T_Y, and T_Z (unequal populations may form through other means, including spin−lattice relaxation). A population with equal sublevel occupations cannot overall absorb or emit RF, precluding observation of an EPR signal. However, individual spins *can*. If one triplet from a geminate triplet pair such as $T_Z + T_Z$ absorbs an RF photon (Figure 5b,c), it transitions to a different sublevel, yielding a mismatch such as $T_Z + T_Y$ that has no overlap with the ^1TT wave function. Reassociation in this case will not form ^1TT or the ^5TT sublevels that couple most strongly to it, Q_{Z^2} and $Q_{X^2-Y^2}$.[4,34] The result is a steady-state reduction in ^1TT population upon RF drive, just as observed in Figure 4.

Unlike the ^1TT-specific PA at 1000 nm, we expect ^1TT and T_1 to show overlapping PA at 600 nm. But just like the NIR-probe PADMR, those PADMR signals are negative as well (Figures 3a and S20). This suggests that the net effect of RF drive is to push population into spin configurations that favor ^3TT—for example, $^3TT_X = 1/\sqrt{2}(|T_YT_Z\rangle - |T_ZT_Y\rangle)$—thus promoting overall triplet population relaxation via TCA (see Figure 5a,c).[36]

https://doi.org/10.1021/acs.jpclett.2c03665
J. Phys. Chem. Lett. 2023, 14, 2387−2394

Thus, our data is consistent with a triplet population dominated by long-lived-spin-correlated geminate triplet pairs that only rarely interact nongeminately. Systems dominated by nongeminate triplet-pair association give the opposite trend, where RF drive increases the rate of triplet fusion.[46,48] This is because nongeminate triplet pair encounters with singlet character may fuse, depleting those configurations from the population at steady state. The result in such a case is that RF drive will push the population toward more singlet pair configurations on average.

It is clear that geminate triplet-pair recombination is dominant in our data, since the 1000 nm probe PADMR signal attributed to ^{1}TT is negative, $-\Delta T/T < 0$. This is not surprising: the low-temperature, low-dimensional transport and large antiferromagnetic J_{TT} would naturally discourage dissociation, slow down diffusion, and encourage reassociation so that the uncoupled T_1 live transiently and rarely diffuse far enough to encounter a nongeminate partner. However, some nongeminate triplet recombination probably does occur, as implied by the shortened PA lifetimes with increased laser intensity (600 nm probe, Figure S13). Since ^{1}TT is probably a trap (lowest energy excited state), it may be surprising that $^1\mathrm{TT} \rightarrow T_1 + T_1$ dissociation would occur at all. But ^{1}TT forms with a large excess of energy (~0.5−1 eV); the time it takes for this energy to dissipate is probably sufficient for some pairs to escape the trap. The excess energy may also be needed to produce the small but observable quintet populations (Figure 3c).

Correlations between PA and MR frequencies. With the data in Figure 4b, we demonstrated a kinetic link between T_1 MR and a PA most likely belonging to ^{1}TT. The $f \times \lambda$-PADMR data also shows that the MR transition frequencies are correlated with the optical absorption wavelengths (Figure 4). Increasing f_{Drive}^{RF} between 960 and 1010 MHz coincides with blue-shifting features in the λ-PADMR spectra. Perhaps most obvious is the sharp superimposed peak that starts at 850 nm (960 MHz) and blue-shifts by as much as 50 nm (90 meV). A similar feature (of opposite sign) is seen in the PA spectrum (Figure 2b) and is likely a GSB. Given that assignment, the positive sign of the superimposed GSB means that the ground-state population is increased by RF drive. The spectral shift is large, but entirely within the expected distribution, given the breadth of the film absorption spectrum (Figure 2a). The implication is that the inhomogeneous broadening in the MR lines and the optical absorptions is related: there is a positive correlation between the optical and magnetic resonance frequencies. Similar behavior is seen when probing the 600 nm PA (Figure S20): high RF-drive frequencies are associated with bluer PA.

Linear correlations between MR and optical line positions have been previously discussed for other triplet states[50−56] and derive from inhomogeneities that perturb the electronic environment. The inhomogeneities must also be relatively static: rapidly sampling different environments produces line-narrowing like is seen with zero-field splittings in solution-phase EPR and NMR spectra. Although we cannot yet identify the specific inhomogeneity responsible, its presence in our data demonstrates an important aspect of PADMR—it is powerfully selective.

In conclusion, we have implemented a new variant of photoinduced-absorption-detected magnetic resonance spectroscopy and used it to study the correlations between magnetic and transient optical spectra in a unique singlet-fission material, polycrystalline TSPS-PDT. We identify strong magnetic resonance transitions associated with uncoupled triplet states, T_1, which are accompanied by weak signatures of coupled ^{5}TT states. Furthermore, we find that the near-infrared photoinduced absorption features previously assigned to a variety of triplet-pair states are correlated with magnetic transitions in the T_1 manifold. These observations are consistently explained by a model where the free triplet population is dominated by spin-correlated geminate triplet pairs, and driving magnetic transitions promotes ^{3}TT configurations that have a rapid relaxation pathway while simultaneously forbidding fusion back to ^{1}TT. We thus assign the near-infrared optical absorption to ^{1}TT in this system.

These results show the long-persistent spin correlations present in this and similar singlet-fission materials at low temperature and demonstrate a unique and versatile way to detect them, even absent net population level spin polarization. While persistent spin correlation is generally useful for quantum information applications, it can be problematic in other applications like triplet state harvesting for photovoltaics, since geminate triplet-pair recombination facilitates deactivation. On the other hand, loss of spin correlation should be accelerated at higher temperatures, possibly mitigating this issue. Outside the context of singlet fission, these studies have laid foundations for detailed understanding of essentially any spin-active excited state through correlations between optical absorption and magnetic resonance.

■ ASSOCIATED CONTENT

Supporting Information

The Supporting Information is available free of charge at https://pubs.acs.org/doi/10.1021/acs.jpclett.2c03665.

Detailed exposition of sample preparation, detailed discussion of all spectroscopic methods, instrument details, data analysis methods, RF coupling loop simulations, supplemental exploration of laser power and magnetic field dependence of the signals, and various supplemental discussions of points discussed more briefly in the main text (PDF)

■ AUTHOR INFORMATION

Corresponding Author

Obadiah G. Reid − *Renewable and Sustainable Energy Institute, University of Colorado, Boulder, Colorado 80309, United States; National Renewable Energy Laboratory, Golden, Colorado 80401, United States;* orcid.org/0000-0003-0646-3981; Email: obadiah.reid@colorado.edu, obadiah.reid@nrel.gov

Authors

Ryan D. Dill − *University of Colorado Boulder, Department of Chemistry, Boulder, Colorado 80309, United States;* orcid.org/0000-0002-0954-6574

Gajadhar Joshi − *National Renewable Energy Laboratory, Golden, Colorado 80401, United States*

Karl J. Thorley − *University of Kentucky Center for Applied Energy Research, Lexington, Kentucky 40511, United States;* orcid.org/0000-0003-0665-3363

John E. Anthony − *University of Kentucky Center for Applied Energy Research, Lexington, Kentucky 40511, United States; Department of Chemistry, University of Kentucky, Lexington, Kentucky 40506, United States;* orcid.org/0000-0002-8972-1888

https://doi.org/10.1021/acs.jpclett.2c03665
J. Phys. Chem. Lett. 2023, 14, 2387−2394

Brian Fluegel − *National Renewable Energy Laboratory, Golden, Colorado 80401, United States*
Justin C. Johnson − *National Renewable Energy Laboratory, Golden, Colorado 80401, United States; Renewable and Sustainable Energy Institute, University of Colorado, Boulder, Colorado 80309, United States;* orcid.org/0000-0002-8874-6637

Complete contact information is available at: https://pubs.acs.org/10.1021/acs.jpclett.2c03665

Notes

The authors declare no competing financial interest.

■ ACKNOWLEDGMENTS

This work was authored in part by the National Renewable Energy Laboratory, operated by Alliance for Sustainable Energy, LLC, for the U.S. Department of Energy (DOE) under Contract No. DE-AC36-08GO28308. Funding was provided by the U.S. Department of Energy, Office of Basic Energy Sciences, Division of Chemical Sciences, Biosciences, and Geosciences. The views expressed in the article do not necessarily represent the views of the DOE or the U.S. Government. The U.S. Government retains and the publisher, by accepting the article for publication, acknowledges that the U.S. Government retains a nonexclusive, paid-up, irrevocable, worldwide license to publish or reproduce the published form of this work, or allow others to do so, for U.S. Government purposes.

■ REFERENCES

(1) Luther, J. M.; Johnson, J. C. An exciting boost for solar cells. *Nature* **2019**, *571*, 38−39.
(2) Hanna, M. C.; Nozik, A. J. Solar conversion efficiency of photovoltaic and photoelectrolysis cells with carrier multiplication absorbers. *J. Appl. Phys.* **2006**, *100*, 074510.
(3) Einzinger, M.; Wu, T.; Kompalla, J. F.; Smith, H. L.; Perkinson, C. F.; Nienhaus, L.; Wieghold, S.; Congreve, D. N.; Kahn, A.; Bawendi, M. G.; Baldo, M. A. Sensitization of silicon by singlet exciton fission in tetracene. *Nature* **2019**, *571*, 90−94.
(4) Smyser, K. E.; Eaves, J. D. Singlet fission for quantum information and quantum computing: the parallel JDE model. *Sci. Rep.* **2020**, *10*, 18480.
(5) Lewis, S. G.; Smyser, K. E.; Eaves, J. D. Clock transitions guard against spin decoherence in singlet fission. *J. Chem. Phys.* **2021**, *155*, 194109.
(6) Jacobberger, R. M.; Qiu, Y.; Williams, M. L.; Krzyaniak, M. D.; Wasielewski, M. R. Using Molecular Design to Enhance the Coherence Time of Quintet Multiexcitons Generated by Singlet Fission in Single Crystals. *J. Am. Chem. Soc.* **2022**, *144*, 2276.
(7) Rugg, B. K.; Smyser, K. E.; Fluegel, B.; Chang, C. H.; Thorley, K. J.; Parkin, S.; Anthony, J. E.; Eaves, J. D.; Johnson, J. C. Triplet-pair spin signatures from macroscopically aligned heteroacenes in an oriented single crystal. *Proc. Natl. Acad. Sci. U. S. A.* **2022**, *119*, e2201879119.
(8) Dill, R. D.; Smyser, K. E.; Damrauer, N. H.; Eaves, J. D. Entangled, Spin-polarized Excitons from Singlet Fission in a Rigid Dimer. *arXiv*, 2022; arXiv:2202.09678 [physics.chem-ph].
(9) Khan, S.; Mazumdar, S. Theory of Transient Excited State Absorptions in Pentacene and Derivatives: Triplet-Triplet Biexciton versus Free Triplets. *J. Phys. Chem. Lett.* **2017**, *8*, 5943−5948.
(10) Pace, N. A.; Rugg, B. K.; Chang, C. H.; Reid, O. G.; Thorley, K. J.; Parkin, S.; Anthony, J. E.; Johnson, J. C. Conversion between triplet pair states is controlled by molecular coupling in pentadithiophene thin films. *Chem. Sci.* **2020**, *11*, 7226−7238.
(11) Goetz, K. P.; Li, Z.; Ward, J. W.; Bougher, C.; Rivnay, J.; Smith, J.; Conrad, B. R.; Parkin, S. R.; Anthopoulos, T. D.; Salleo, A.; Anthony, J. E.; Jurchescu, O. D. Effect of Acene Length on Electronic Properties in 5-, 6-, and 7-Ringed Heteroacenes. *Adv. Mater.* **2011**, *23*, 3698−3703.
(12) Shinar, J. Optically detected magnetic resonance studies of luminescence-quenching processes in π-conjugated materials and organic light-emitting devices. *Laser Photon. Rev.* **2012**, *6*, 767−786.
(13) Yang, C. G.; Ehrenfreund, E.; Wohlgenannt, M.; Vardeny, Z. V. Comment on "Frequency response and origin of the spin-1/2 photoluminescence-detected magnetic resonance in a π-conjugated polymer. *Phys. Rev. B* **2007**, *75*, 246201.
(14) Wohlgenannt, M.; Jiang, X. M.; Vardeny, Z. V.; Janssen, R. A. Conjugation-Length Dependence of Spin-Dependent Exciton Formation Rates in π-Conjugated Oligomers and Polymers. *Phys. Rev. Lett.* **2002**, *88*, 197401.
(15) Wohlgenannt, M.; Yang, C.; Vardeny, Z. V. Spin-dependent delayed luminescence from nongeminate pairs of polarons in -conjugated polymers. *Phys. Rev. B* **2002**, *66*, 241201.
(16) Wohlgenannt, M.; Tandon, K.; Mazumdar, S.; Ramasesha, S.; Vardeny, Z. V. Formation cross-sections of singlet and triplet excitons in π-conjugated polymers. *Nature* **2001**, *409*, 494−497.
(17) List, E. J.; Kim, C. H.; Naik, A. K.; Scherf, U.; Leising, G.; Graupner, W.; Shinar, J. Interaction of singlet excitons with polarons in wide band-gap organic semiconductors: A quantitative study. *Phys. Rev. B - Condens. Matter Mater. Phys.* **2001**, *64*, 155204.
(18) Wohlgenannt, M.; Graupner, W.; Leising, G.; Vardeny, Z. V. Photogeneration and recombination processes of neutral and charged excitations in films of a ladder-type poly(para-phenylene). *Phys. Rev. B* **1999**, *60*, 5321−5330.
(19) Lane, P.; Wei, X.; Vardeny, Z. Spin and spectral signatures of polaron pairs in π-conjugated polymers. *Phys. Rev. B - Condens. Matter Mater. Phys.* **1997**, *56*, 4626−4637.
(20) Schultz, N.; Vardeny, Z. V.; Taylor, P. C. Optically detected magnetic resonance studies of undoped a-Si:H. *Mater. Res. Soc. Symp. - Proc.* **1996**, *420*, 593−598.
(21) Lane, P. A.; Wei, X.; Vardeny, Z. V.; Poplawski, J.; Ehrenfreund, E.; Ibrahim, M.; Frank, A. J. Spin signature of photoexcitations in sexithiophene. *Synth. Met.* **1996**, *76*, 57−60.
(22) Wei, X.; Vardeny, Z.; Sariciftci, N.; Heeger, A. Absorption-detected magnetic-resonance studies of photoexcitations in conjugated-polymer composites. *Phys. Rev. B* **1996**, *53*, 2187−2190.
(23) Wei, X.; Hess, B. C.; Vardeny, Z. V.; Wudl, F. Studies of photoexcited states in polyacetylene and poly-(paraphenylenevinylene) by absorption detected magnetic resonance: The case of neutral photoexcitations. *Phys. Rev. Lett.* **1992**, *68*, 666−669.
(24) Hoff, A. J., Ed. *Advanced EPR: Applications in Biology and Biochemistry*, 1st ed.; Elsevier Science Publishers B.V.: Amsterdam, 1989.
(25) Clarke, R. H.; Harris, G.; R. A. Mushlint, N. L. TRIPLET STATE PROPERTIES OF POLYCYCLIC AROMATIC HYDROCARBON-DNA and PORPHYRIN-DNA COMPLEXES DETERMINED BY OPTICALLY DETECTED ZERO FIELD MAGNETIC RESONANCE. *Photochem. Photobiol.* **1983**, *37*, 9−15.
(26) Clarke, R. H., Ed. *Triplet State ODMR Spectroscopy: Techniques and Applications to Biophysical Systems*; John Wiley and Sons, Inc., 1982.
(27) Brenner, H. C. Methods for optical detection of electron spin coherence in nonphosphorescent triplet states. *J. Chem. Phys.* **1977**, *67*, 4719−4725.
(28) Clarke, R. H.; Hayes, J. M. Microwave-induced triplet-triplet absorption in organic molecules. *J. Chem. Phys.* **1973**, *59*, 3113−3118.
(29) Clarke, R. H.; Hayes, J. M. Triplet state dynamics in polycyclic aromatic molecules. *Chem. Phys. Lett.* **1974**, *27*, 556−561.
(30) Clarke, R. H.; Connors, R. E. An investigation of the triplet state dynamics of zinc chlorophyll b by microwave-induced changes in the intensity of fluorescence and singlet-singlet absorption. *Chem. Phys. Lett.* **1975**, *33*, 365−368.

(31) Tuan Trinh, M.; Pinkard, A.; Pun, A. B.; Sanders, S. N.; Kumarasamy, E.; Sfeir, M. Y.; Campos, L. M.; Roy, X.; Zhu, X. Y. Distinct properties of the triplet pair state from singlet fission. *Sci. Adv.* **2017**, *3*, e1700241.
(32) Miyata, K.; Conrad-Burton, F. S.; Geyer, F. L.; Zhu, X. Y. Triplet Pair States in Singlet Fission. *Chem. Rev.* **2019**, *119*, 4261−4292.
(33) Yarmus, L.; Rosenthal, J.; Chopp, M. EPR of triplet excitons in tetracene crystals: spin polarization and the role of singlet exciton fission. *Chem. Phys. Lett.* **1972**, *16*, 477−481.
(34) Benk, H.; Sixl, H. Theory of two coupled triplet states. *Mol. Phys.* **1981**, *42*, 779−801.
(35) Weil, J. A.; Bolton, J. R.; Wertz, J. E. *Electron Paramagnetic Resonance: elementary theory and practical applications*, 1st ed.; John Wiley and Sons, Inc, 1994.
(36) Merrifield, R. E. Magnetic effects on triplet exciton interactions. *Pure Appl. Chem.* **1971**, *27*, 481−498.
(37) Groff, R.; Merrifield, R.; Avakian, P. Singlet and triplet channels for triplet-exciton fusion in anthracene crystals. *Chem. Phys. Lett.* **1970**, *5*, 168−170.
(38) Chen, M.; et al. Quintet-triplet mixing determines the fate of the multiexciton state produced by singlet fission in a terrylenediimide dimer at room temperature. *Proc. Natl. Acad. Sci. U. S. A.* **2019**, *116*, 8178−8183.
(39) Yago, T.; Tashiro, M.; Hasegawa, K.; Gohdo, M.; Tsuchiya, S.; Ikoma, T.; Wakasa, M. Triplet-Triplet Annihilation via the Triplet Channel in Crystalline 9,10-Diphenylanthracene. *J. Phys. Chem. Lett.* **2022**, *13*, 8768−8774.
(40) Johnson, R. C.; Merrifield, R. E. Effects of Magnetic Fields on the Mutual Annihilation of Triplet Excitons in Anthracene Crystals. *Phys. Rev. B* **1970**, *1*, 896−902.
(41) Carrington, A., McLachlan, A. D. *Introduction to Magnetic Resonance With Applications to Chemistry and Chemical Physics*; Harper and Row: New York, 1967; pp 118−119.
(42) Schwoerer, M.; Huber, R. A.; Hartl, W. Quintet states of organic molecules: magnetic energies, spin-states and ESR-selection rules. *Chem. Phys.* **1981**, *55*, 97−102.
(43) Lubert-Perquel, D.; Salvadori, E.; Dyson, M.; Stavrinou, P. N.; Montis, R.; Nagashima, H.; Kobori, Y.; Heutz, S.; Kay, C. W. Identifying triplet pathways in dilute pentacene films. *Nat. Commun.* **2018**, *9*, 4222.
(44) Tayebjee, M. J. Y.; Sanders, S. N.; Kumarasamy, E.; Campos, L. M.; Sfeir, M. Y.; McCamey, D. R. Quintet multiexciton dynamics in singlet fission. *Nat. Phys.* **2017**, *13*, 182−188.
(45) Yunusova, K. M.; Bayliss, S. L.; Chanelière, T.; Derkach, V.; Anthony, J. E.; Chepelianskii, A. D.; Weiss, L. R. Spin Fine Structure Reveals Biexciton Geometry in an Organic Semiconductor. *Phys. Rev. Lett.* **2020**, *125*, 097402.
(46) Bayliss, S. L.; Chepelianskii, A. D.; Sepe, A.; Walker, B. J.; Ehrler, B.; Bruzek, M. J.; Anthony, J. E.; Greenham, N. C. Geminate and nongeminate recombination of triplet excitons formed by singlet fission. *Phys. Rev. Lett.* **2014**, *112*, 238701.
(47) Budden, P. J.; Weiss, L. R.; Müller, M.; Panjwani, N. A.; Dowland, S.; Allardice, J. R.; Ganschow, M.; Freudenberg, J.; Behrends, J.; Bunz, U. H. F.; Friend, R. H. Singlet exciton fission in a modified acene with improved stability and high photoluminescence yield. *Nat. Commun.* **2021**, *12*, 1527.
(48) Joshi, G.; Dill, R. D.; Thorley, K. J.; Anthony, J. E.; Reid, O. G.; Johnson, J. C. Optical readout of singlet fission biexcitons in a heteroacene with photoluminescence detected magnetic resonance. *J. Chem. Phys.* **2022**, *157*, 164702.
(49) Smith, M. B.; Michl, J. Singlet Fission. *Chem. Rev.* **2010**, *110*, 6891−6936.
(50) Williamson, R. L.; Kwiram, A. L. On the nature of the relationship between inhomogeneously broadened phosphorescence and ODMR spectral lines. *J. Chem. Phys.* **1988**, *88*, 6092−6106.
(51) Loboda, O.; Minaev, B.; Vahtras, O.; Ruud, K.; Agren, H. Ab initio study of nonhomogeneous broadening of the zero-field splitting of triplet guest molecules in diluted glasses. *J. Chem. Phys.* **2003**, *119*, 3120−3129.
(52) Gradl, G.; Friedrich, J. Investigation of inhomogeneous line broadening of ODMR transitions in doped organic glasses. *Chem. Phys. Lett.* **1985**, *114*, 543−546.
(53) Clark, S.; Tinti, D. Relationship of the inhomogeneous broadenings in the triplet state optical and ODMR spectra of NaNO2/Ag+. *Chem. Phys.* **1980**, *51*, 17−30.
(54) Kwiram, A. L.; Alexander Ross, J.; Deranleau, D. A. Wavelength dependence of the zero-field splittings in the triplet state of tryptophan. *Chem. Phys. Lett.* **1978**, *54*, 506−509.
(55) Lemaistre, J.; Zewail, A. On the inhomogeneous and homogeneous broadenings of optical and ODMR transitions of triplet states in solids. *Chem. Phys. Lett.* **1979**, *68*, 296−301.
(56) Van Egmond, J.; Kohler, B. E.; Chan, I. Solvent shift broadening in the PMDR spectrum of quinoxaline. *Chem. Phys. Lett.* **1975**, *34*, 423−426.

https://doi.org/10.1021/acs.jpclett.2c03665
J. Phys. Chem. Lett. 2023, 14, 2387−2394